Formation of Sub-100 nm Femtosecond Laser-Induced Periodic Fine Structures on Laser Powder Bed Fusion Fabricated Stainless Steel

Chung-Wei Cheng*, Siou-Jhun Jhu, Yi-Hsien Liu, and Shu-Chun Yeh

Department of Mechanical Engineering, National Yang Ming Chiao Tung University, No. 1001, Ta Hsueh Road, Hsinchu 300, Taiwan
** Corresponding author's e-mail: weicheng@nycu.edu.tw*

This study investigated laser-induced periodic surface structures (LIPSS) produced on laser powder bed fusion (LPBF) fabricated SUS316L (LPBF-SUS) and typical cold-rolled SUS 304 (CR-SUS) by femtosecond fiber laser with a wavelength of 515 nm. The HSFL (high spatial frequency LIPSS) appeared related to CR-SUS grain boundary characteristics and was partially formed. In addition, the uniform HSFL on the LPBF-SUS with a period of about 60~70 nm (~λ/8) was demonstrated.
DOI: 10.2961/jlmn.2023.01.2006
Keywords: laser processing, grain boundaries, laser-induced periodic surface structure, laser powder bed fusion

1. Introduction

Laser-induced periodic surface structures (LIPSS) can create LSFL (low spatial frequency LIPSS) and HSFL (high spatial frequency LIPSS) through femtosecond beam laser scanning [1-3]. The period of LSFL is close to the laser wavelength ($\Lambda_{LSFL} \leq \lambda$), and the period of HSFL is less than half the laser wavelength ($\Lambda_{HSFL} < \lambda/2$). The novel structures can be used to change the physical properties of the material surface [2].

Stainless steel is one of the most commonly used alloy materials in the industry and medical devices due to its good corrosion resistance. Numerous researchers have recently fabricated HSFL, LSFL, and hybrid structures on stainless steel surface by pico- or femtosecond laser [4-7]. Kietzig et al. [4] used a femtosecond laser to fabricate a dual-scale structure on the stainless steel, and found that the treated surface has superhydrophobic properties. Römer et al. [5] used an 800 nm femtosecond laser to fabricate LSFL structure (300~500 nm) and found regular ripples (~150 nm) on the grain boundary of AISI 316 material. Gecys et al. [6] used a femtosecond laser at 515 nm to fabricate the LSFL structure (~400 nm) and HSFL structure (250~300 nm) on the stainless steel. Ding et al. [7] used a picosecond laser with a laser wavelength of 515 nm to fabricate LSFL and HSFL structures on a conventional 316L stainless steel sheet. It was observed that the HSFL structure was incompletely formed on an irradiated surface.

Metal parts fabricated by the laser powder bed fusion (LPBF) process followed by the femtosecond surface treatment have been published recently. Mingareev et al. [8] used femtosecond laser ablation for surface treatment of LPBF fabricated nickel-based alloy components and found that the surface roughness can be reduced. Cheng et al. [9] used a picosecond laser to fabricate LSFL structure on LPBF Ti6Al4V parts and improve its hydrophobicity. Ghosh et al. [10] fabricated grooves on the LPBF fabricated stainless steel parts by femtosecond laser, and LSFL was found on the groove. Ackerl et al. [11] fabricated LIPSS and cone-like protrusions on the LPBF stainless steel parts using a picosecond laser. It was found that LSFL generated depends on grain orientation and boundary defects during the ablation process. Note that due to the laser scanning pattern and the rapid cooling of the liquid metal during the LPBF process, the parts have different molten pool grain boundaries and sub-grain microstructures [12]. For LPBF-fabricated stainless steel components, the current research only discusses LSFL [11], but there is no literature research on HSFL.

In this study, a femtosecond laser with a wavelength of 515 nm was used to irradiate the stainless steel components manufactured by two different processes, cold-rolled SUS 304 (CR-SUS) and laser powder bed fusion (LPBF) fabricated SUS316L (LPBF-SUS). The morphology produced by LSFL and HSFL is discussed.

2. Materials and methods

The cold-rolled SUS 304 (CR-SUS) and LPBF fabricated stainless steel 316L parts (LPBF-SUS) were nanostructured in the air with a femtosecond laser. Fig. 1 shows the schematic setup of the processing system. The femtosecond fiber laser (KASMORO, mRadian Inc.) had a wavelength of 1030 nm, a pulse duration of 420 fs, a repetition rate of 100 kHz, and a maximum laser power of 2 W. The laser beam was linearly polarized and passed through the BBO crystal to convert the laser beam with a wavelength of 515 nm and beam diameter of 1.7 mm ($1/e^2$). The laser beam was then expanded to 3.4 mm by an expander (magnification 2x) and converted to a top-hat profile by a beam shaper (FBS2, TOPAG). The transmitted beam passed through a series of mirrors, entered a galvanometric scanner, and focused on the specimen surface by an F-theta lens (focal length 165 mm). The focal square top hat width (at $1/e^2$) was approximately 50 μm.

LPBF-SUS specimen (Fig. 1)(c)) with size 10 x 10 x 10 mm^3 was fabricated from stainless steel metal powder (316L, Chung Yo Materials) with LPBF equipment (ITRI

AM100). The process parameters are powder layer thickness of 30 μm, laser power of 150 W, and scanning speed of 1200 mm/s. The LPBF-SUS is ground and polished to reduce the surface roughness to Ra <100 nm.

The surface morphology is analyzed through optical microscope (OM) and scanning electron microscope (SEM, Hitachi SU-8010). In addition, a metallographic analysis was performed on the specimen. The specimen was etched using the ten percent oxalic acid etch test for stainless steel (according to the GBT 4334-2008 standard). The solution temperature was 50°C, the current was 1 A, and the corrosion time for CR-SUS and LPBF-SUS was 3 min and 0.5 min, respectively. Fig. 2 shows the metallographic images of CR-SUS and LPBF-SUS before laser treatment, respectively. CR-SUS has a grain size of about 20-40 μm, while LPBF-SUS has a grain size of 10-20 μm. From the magnified images, as shown in Fig. 2(d), it was found that the LPBF-SUS comprises cellular and dendrites structures.

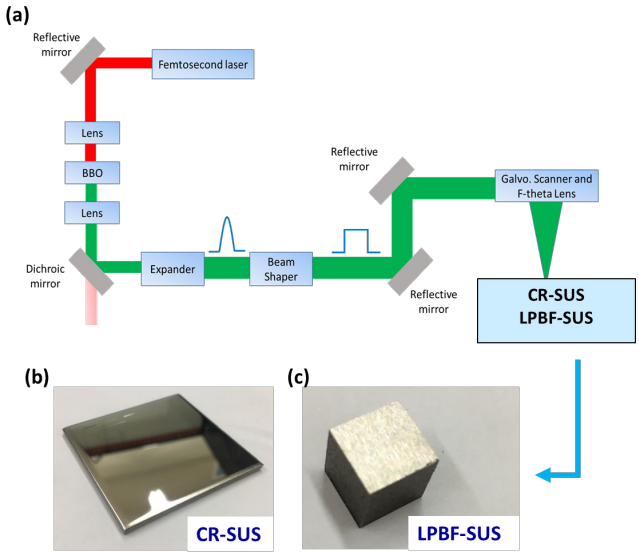

Fig. 1 Schematic setup of the processing system.

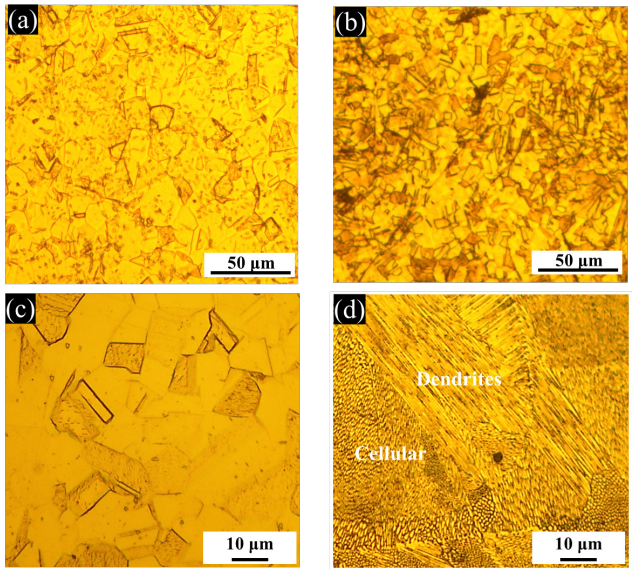

Fig. 2 Metallographic image before laser treatment: (a) CR-SUS, (b) LPBF-SUS, (c)(d) magnified images of (a)(b), respectively.

3. Results and Discussions

Fig. 3 shows the SEM images of CR-SUS and LPBF-SUS materials irradiated by the stationary beam (percussion irradiation) with 75 pulses and different laser power. In both materials, as shown in Fig. 3(a)(c), it can be seen that the LSFL with a period of 400~450 nm was generated, and the LSFL orientation is approximately perpendicular to polarization (E). As the laser power decreased, as shown in Fig. 3(b)(d), the LSFL almost disappeared. From the magnified images, the HSFL with a period of about 60~70 nm (~λ/8, see Fig. 3(e)(g)) was generated, and HSFL orientation is approximately parallel to polarization (E). Fig. 3(b) shows the two forms of HSFL on gray and black distinct areas of CR-SUS, i.e., HSFL-1 (typical HSFL) and HSFL-2. The HSFL-2 shows an unobvious pattern (see Fig. 3(f)). For LPBF-SUS material, as shown in Fig. 3(g)(h), the uniform HSFL can be obtained in the irradiation area.

The LSFL and HSFL periods are similar to the previous research that used a picosecond laser (515 nm) to fabricate LSFL (356±17 nm) and HSFL (58±15 nm) structures on 316L stainless steel [7]. The formation of LSFL can be explained by the optical interference of the incident laser beam and the excited surface plasmon wave [13]. On the other hand, the HSFL may be attributed to the second and higher harmonic generation [14] and cavitation instabilities [15]. In addition, the grain boundary of CR-SUS could explain the selective formation of different HSFL, which might cause inhomogeneous absorption of the laser energy. Therefore, the periodic nano-ripples will be first generated at the grain boundary of stainless steel material [5].

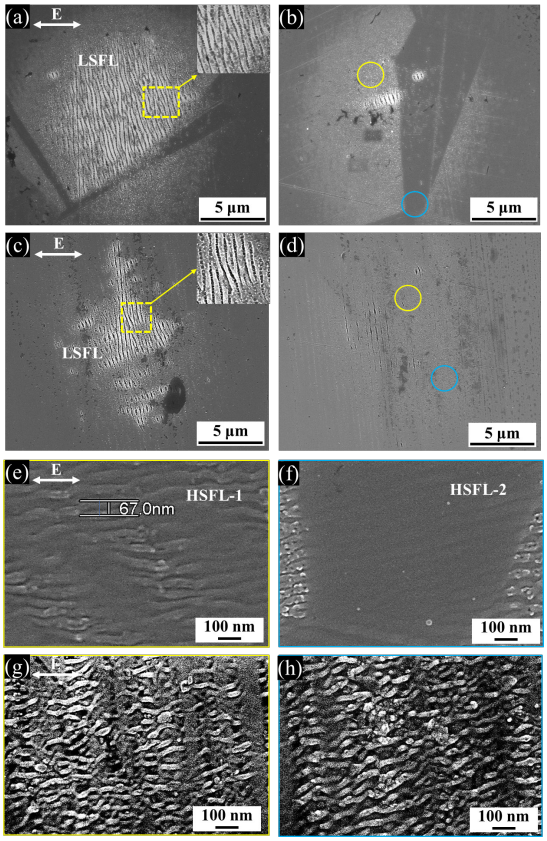

Fig. 3 SEM images of (a)(b) CR-SUS and (c)(d) LPBF-SUS irradiated by stationary beam with the number of shots 75, and different laser power: (a) 75 mW, (b) 65 mW, (c) 55 mW, (d) 50 mW. (e)-(h) magnified images of the circles (yellow, blue) shown in (b)(d), respectively.

Fig. 4 shows the SEM images of CR-SUS irradiated by the Zig-Zag scanning with a scanning speed of 20 mm/s, laser power of 65 mW, hatch distance of 20 μm, and a scanning direction parallel to the laser polarization. In Fig. 4(a), it was found that many gray and black areas were adjacently connected (similar to Fig. 3(b)). In Fig. 4(b), HSFL-1 and HSFL-2 are shown on both sides of the block boundary. It was found that the fabricated HSFL structures vary with the crystal orientation planes of the material. Fig. 4(c) shows the SEM images (tilt angle 30°). It was found that there was a slight height difference between HSFL-1 and HSFL-2. EDS analysis was conducted to measure the chemical composition of the different HSFL nanostructures. The EDS spectrum and the atomic percentages of HSFL-1 are shown in Fig. 4(d). Table 1 is a comparison of the material composition of HSFL-1 and HSFL-2. The material composition ratio is slightly different. In [7], they found that the HSFL formation area by picosecond laser is influenced by the metallic grain of 316L stainless steel. HSFL preferentially occurs in the interior grains with low surface atomic planar densities. This study used a femtosecond laser to irradiate cold-rolled 304 stainless steel and also found this phenomenon.

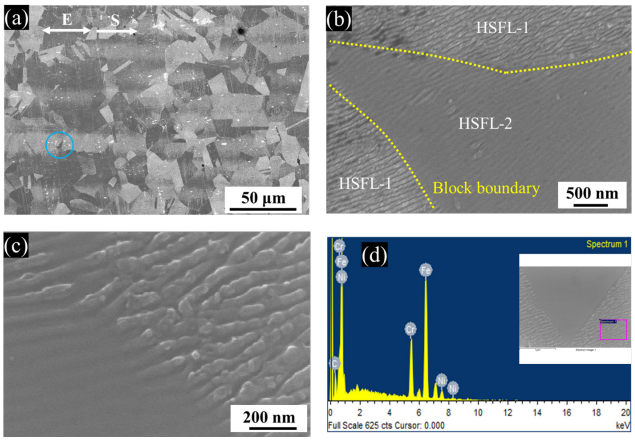

Fig. 4 (a) area pattern of CR-SUS irradiated by a scanning laser beam, (b) magnified images of the blue circle in (a), (c) SEM tilt angle (30°), and (d) EDS analysis of the HSFL-1.

Table 1 Atomic percentages of different HSFL structures.

Structure	Fe	Cr	Ni
HSFL-1	46.67	13.79	5.23
HSFL-2	50.14	14.98	5.73

Fig. 5 shows the HSFL structures on the LPBF-SUS material fabricated by femtosecond laser scanning. From the magnified images of the four areas in Fig. 5(a), it can be found that the HSFL was uniformly generated. In Fig. 5(a), the HSFL is generated in the scanning area (black color), and the gray regions are LSFL. The HSFL forming area is not affected by the material grain boundaries. The distribution of LSFL in some regions is mainly due to the LPBF-SUS surface is not mirror-polished, and the local area has high roughness, resulting in LSFL [11] or grain orientation and boundary defects [11].

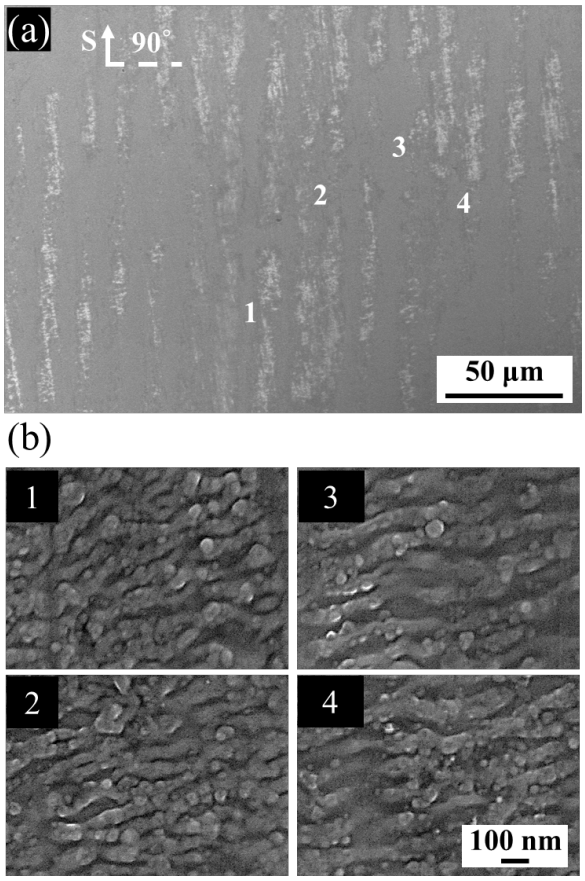

Fig. 5 (a) area pattern of LPBF-SUS irradiated by femtosecond laser scanning. (b) 1-4 magnified images of the mark shown in (a), respectively.

Fig. 6 shows the HSFL structures on the LPBF-SUS material fabricated by femtosecond laser scanning with directions 30˚and 60˚, respectively. HSFL is also almost uniformly generated in the scanning area, and a few gray areas are LSFL. In magnified images, the HSFL orientation is usually parallel to polarization as the scanning direction changes. It can be inferred that the forming of HSFL will not be affected by the trajectory of the LPBF molten pool.

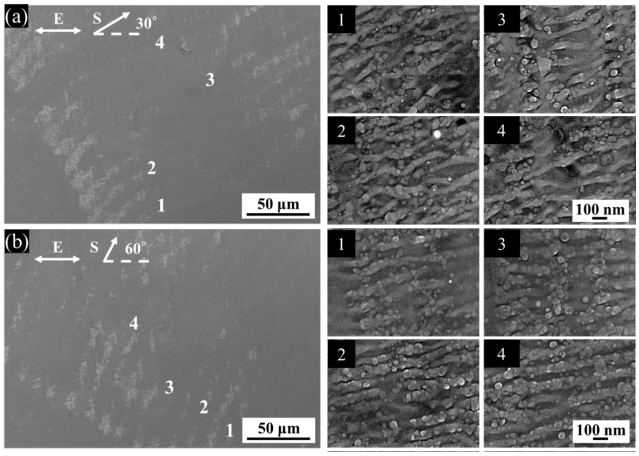

Fig. 6 Area pattern of LPBF-SUS irradiated by femtosecond laser with scanning direction (a)30˚, (b)60˚. 1-4 magnified images of the mark shown in (a)(b), respectively.

4. Conclusion

This study investigated linearly polarized femtosecond laser beams with 515 nm irradiated on cold-rolled SUS 304 (CR-SUS) and LPBF fabricated stainless steel 316L (LPBF-SUS) parts. The experimental results demonstrated that two different HSFLs were generated on CR-SUS materials, i.e., typical HSFL and unobvious HSFL; The grain boundary could explain the selective formation of different HSFL on the CR-SUS might cause inhomogeneous absorption of the laser energy. HSFL is almost uniformly generated on the LPBF-SUS parts. Besides, the forming of HSFL will not be affected by the LPBF molten pool.

Acknowledgments

This work was supported by the Ministry of Science and Technology of Republic of China, under Contract MOST 110-2221-E-A49-110 and 110-2218-E-006-028.

References

[1] A. Y. Vorobyev and C. Guo: Laser Phys. Lett., 3, (2013) 385.
[2] J. Bonse, S. Höhm, S. V. Kirner, A. Rosenfeld, and J. Krüger: IEEE J. Sel. Top. Quantum Electron., 3, (2017) 9000615.
[3] C. Florian, S. V. Kirner, J. Krüger, and J. Bonse: J. Laser Appl., 2, (2020) 022063.
[4] A. M. Kietzig, S. Hatzikiriakos, and P. Englezos: Langmuir., 25, (2009) 4821.
[5] G. Römer, A. Huis, J. Meijer, and M. Groenendijk: CIRP annals., 1, (2009) 201.
[6] P. Gecys: J. Laser Micro/Nanoeng., 10, (2015) 129.
[7] S. Ding, D. Zhu, W. Xue, W. Liu, and Y. Cao: Nanomaterials., 1, (2020) 62.
[8] I. Mingareev, T. Bonhoff, A.F. El-Sherif, W. Meiners, I. Kelbassa, T. Biermann, and M. Richardson.: J. Laser Appl., 5, (2013) 052009.
[9] C. W. Cheng, C. W. Chien, D. Y. Lin, and J. B. Horng: CJME., 6, (2015) 543.
[10]A. Ghosh, X. Wang, A.-M. Kietzig, and M. Brochu: J. Manuf. Processes., 35, (2018) 327.
[11]N. Ackerl, G. Fisch, J. Auerswald, and K. Wegener: SN Appl. Sci., 4, (2020) 1.
[12]D. Herzog, V. Seyda, E. Wycisk, and C. Emmelmann: Acta Mater., (2016) 371.
[13]M. Huang, F. Zhao, Y. Cheng, N. Xu, and Z. Xu: ACS Nano., 12, (2009) 4062.
[14]X.-F. Li, C.-Y. Zhang, H. Li, Q.-F. Dai, S. Lan, and S.-L. Tie: Opt. Express., 23, (2014) 28086.
[15]A.A. Ionin, S.I. Kudryashov, S.V. Makarov, L.V. Seleznev, D.V. Sinitsyn, A.E. Ligachev, E.V. Golosov, and Y.R. Kolobov: Laser Phys. Lett., 5, (2013) 056004.

(Received: June 17, 2022, Accepted: February 15, 2023)